Available online at www.sciencedirect.com
ScienceDirect
Polymer 47 (2006) 7519–7534
polymer
www.elsevier.com/locate/polymer

Gas permeation in poly(ether imide) nanocomposite membranes based on surface-treated silica. Part 1: Without chemical coupling to matrix

S. Takahashi [a,b], D.R. Paul [a,b,*]

[a] Department of Chemical Engineering, The University of Texas at Austin, Austin, TX 78712-1062, USA
[b] Texas Materials Institute, The University of Texas at Austin, Austin, TX 78712-1062, USA

Received 14 July 2006; received in revised form 15 August 2006; accepted 15 August 2006
Available online 11 September 2006

Abstract

The long range objective of this research is to understand to what extent the presence of nanosized particles may change the local properties, and specifically permselectivity characteristics, of a glassy polymer matrix or whether conventional composite theory can be applied to such composites, i.e., the matrix properties are not changed by the filler. In this work, nanocomposite membranes based on an amorphous, glassy poly(ether imide) were formed by incorporating three kinds of hydrophobically treated fumed silica by solution casting and melt processing techniques. However, there is considerable evidence that these nanocomposites contain voids or defects, probably at the polymer–particle interface or within aggregates, that increase gas permeability and decrease selectivity. Thus, the primary focus of this paper is the relation between the extent of voids formed in the nanocomposite and the permeation properties. In addition, this paper deals with techniques for dispersing nanosized particles, fumed silica, in the polymer matrix, characterization of morphology of this mixture using TEM and SEM, and evaluation of local properties based on gas permeation.

Keywords: Nanocomposites; Silica; Permeation

1. Introduction

Polymer composite membranes and barrier films have attracted much interest in recent years; some of the reasons can be easily understood in terms of composite theory particularly for cases where the filler has a high aspect ratio. Composite theories assume that the properties of each phase are the same as if the other phase were not there; however, very near the surface of filler particles, the polymer chain packing and dynamics may be altered. This makes very little impact on overall performance when the particles are large. As the particles become much smaller, on the other hand, the amount of surface area increases and the distance between particles decreases. In this case, effects of the interface may become very important and the matrix phase effectively may not behave as it does in the bulk. The particles of interest may be in the form of spheres, rods and platelets of which fumed silica, carbon nanotubes, and clays are examples. Another interesting case is where the particles are permeable but highly selective, like zeolites, and may improve the selectivity of the composite, i.e., so-called ‘‘mixed matrix membranes’’ [1–8]; however, performance of such composite membranes often seems to be compromised by the formation of voids or defects caused by dewetting of the polymer at the surface of the zeolite particles [1–8]. These problems have hindered the development of such membrane materials. Polymers filled with nanosized particles often show filler agglomeration and network formation in the polymer matrix. Agglomeration may make performance worse than that of the matrix polymer. To resolve nanoparticle agglomeration or defects and improve the filler particle dispersion in the matrix, a great deal of attention has been devoted to modify the interface between the filler and the matrix polymer [1–13].

* Corresponding author. Department of Chemical Engineering, The University of Texas at Austin, Austin, TX 7812-1062, USA. Tel.: +1 512 471 5392; fax: +1 512 471 0542.
E-mail address: drp@che.utexas.edu (D.R. Paul).

0032-3861/$ - see front matter © 2006 Elsevier Ltd. All rights reserved.
doi:10.1016/j.polymer.2006.08.029

Recently, Freeman, Merkel et al. have shown marked deviation from expected permeation behavior for high free volume polymers, e.g., poly(4-methyl-2-pentyne) (PMP) or poly (2,2-bis(trifluoromethyl)-4,5-difluoro-1,3-dioxole-*co*-tetrafluoroethylene), containing silica particles [14–19]. Pinnau et al. have investigated organic-vapor–gas separation properties of PMP membranes containing silica particles [20,21]. They have shown that addition of fumed silica particles to a high free volume polymer, i.e., rigid chain polyacetylene, increases the absolute permeability to penetrant molecules and increases the selectivity of *n*-butane relative to methane. Their work was motivated by an interest in developing better membranes for separation processes. These are very provocative results that clearly indicate permeation in nanocomposites is a fertile area for both fundamental research and possibly for useful applications. Their work suggests that chain rigidity of the matrix polymer may be a key parameter to explore. Thus, the purpose here is to explore whether these effects exist in more conventional polymers. In the present work, we report on the properties and structure of composite membranes formed from impermeable silica particles and an amorphous engineering plastic, ULTEM®; see structure in Fig. 1. This amorphous polymer has high heat resistance, strength, modulus, inherent flame resistance with low smoke evolution plus other attributes; in addition, it is amenable to conventional melt processing [22]. This material and its nanocomposites may have a variety of structural applications [22] in addition to possible uses as a membrane [23]. Moreover, the imide rings of ULTEM® are capable of linking nanosized filler particles via appropriate coupling agents. Thus, this material has many advantages for the current investigation. The objective of this research is to determine whether the presence of nanosized particles changes the permeability and selectivity characteristics of a glassy polymer matrix or if conventional composite theory can be applied to composites containing nano-scale particles. This paper deals with techniques for dispersing fumed silica in the polymer matrix, characterization of morphology of this mixture, and evaluation of local properties

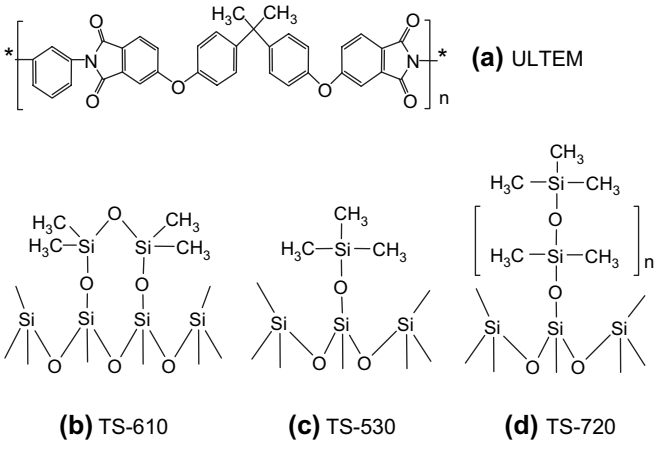

Fig. 1. Chemical structures of the materials used in this study. (a) Poly(ether imide) (ULTEM®), (b) fumed silica with methyl group treatment (TS610), (c) fumed silica with trimethylsilyl group treatment (TS530), and fumed silica with PDMS treatment (TS720) (d).

based on gas permeation. However, a key issue in the current work is that voids or defects at the polymer–particle interface or within agglomerates became an overriding issue that must be addressed. The bulk of this paper deals with approaches to this issue. A subsequent paper will address the use of chemical reactions at the interface as an approach for minimizing interfacial voids or defects.

2. Background

The permeation process of interest here occurs by a solution-diffusion mechanism [24]; i.e., the penetrant sorbs into the polymer at one surface, diffuses through the film, and desorbs from the opposite surface. However, the presence of voids and defects can lead to other mechanisms of transport. The simple solution-diffusion description of the steady-state transport of a penetrant in a homogeneous polymer matrix without voids or defects indicates that the permeability coefficient, P, is the product of the Henry's law solubility coefficient, S, and the diffusion coefficient, D, i.e.,

$$P = DS \tag{1}$$

A similar form has been assumed to apply for composites comprising particles, which do not sorb or conduct the penetrant, dispersed in a matrix whose local characteristics are assumed to be unaffected by the presence of the particles. The latter assertion is an assumption of ''composite theory'' and its validity should be tested when the particles are very small or have a high surface to volume ratio as is the case for so-called ''nanocomposites''.

A simple composite theory for the type of systems mentioned above, in the absence of any solubility in the filler, adsorption on its surface or effects of the filler on the surrounding polymer matrix, would predict the penetrant solubility coefficient for the composite to be [25]

$$S = S_0(1 - \phi) \tag{2}$$

where S_0 is the penetrant solubility coefficient in the pure polymer matrix and ϕ is the volume fraction of the particles dispersed in the matrix. In this approximation, the solubility does not depend on the morphological features of the phases. However, the diffusion process is more complex. The particles are assumed to act as impenetrable barriers so that the penetrant must follow an elongated, or tortuous, path in order to diffuse through the composite [25]. This can be accounted for by a tortuosity factor, f

$$D = D_0 f \tag{3}$$

According to simple composite theory, this tortuosity factor depends on the content of particles, ϕ; the particle shape, e.g., an aspect ratio, α; and the location and orientation of the particles in space; however, it should not depend on absolute particle size or what the penetrant is. Combining the above equations gives

$$P = DS = (1 - \phi)S_0 D_0 f = (1 - \phi)P_0 f \tag{4}$$

where P_0 is the penetrant permeability coefficient in the pure polymer matrix. In principle, this impedance or tortuosity factor, f, can be calculated by an appropriate solution to Fick's law if a complete description of the two-phase morphology is known. There is an extensive literature devoted to this problem using varying approaches and levels of sophistication or approximation [26–36]. One of the first examples was Maxwell's theory which predicts f for spherical particles [26]

$$f = \left(1 + \frac{\phi}{2}\right)^{-1} \tag{5}$$

The predicted f for a composite containing periodically arrayed infinite cylinders is [27]

$$f = (1 + \phi)^{-1} \tag{6}$$

Nielsen assumed a specific regular array of platelets or ribbons of aspect ratio $\alpha = l/w$ (l = length and w = width of platelets) [28] and obtained

$$f = \left(1 + \frac{1}{2}\alpha\phi\right)^{-1} \tag{7}$$

Other theories for arrayed platelets or ribbons have been proposed based on various types of analysis [29–36].

It is useful to examine the literature on permeation in composites and nanocomposites to see if there is evidence for or against the validity of the local property assumption inherent in composite theory. Some of the pioneering research by Barrer et al. on permeation in polymers included measurements on rubbery polymers containing inorganic fillers like zinc oxide and silica [37,38]. These papers don't give a complete characterization of the filler particles used, but the information available indicates they are a few microns in dimension and are much larger than the nano-scale particles of interest here. A careful analysis of the available data suggests that the results are in reasonable accord with the predictions of composite theory [38] as might be expected for such large particles and the corresponding low surface to volume ratio. However, the data do show some evidence for voids at the particle interface because of either poor wetting by the polymer or processing issues.

3. Experimental

3.1. Materials and film preparation

Three fumed silica materials commercially available from Cabot Corp. were used as fillers in this study; they are described in Fig. 1. Each of these products was chemically treated by reacting surface hydroxyl groups on the hydrophilically fumed silica to give the type of surface chemistries suggested in Fig. 1 [39]. Such treatments make fumed silica hydrophobic; these fillers have different surface area and particle diameters as shown in Table 1 [39]. The polymer used in this study is poly(ether imide) resin ULTEM® 1000 from GE Plastics. Nanocomposite membranes with thicknesses in the range of 50–70 μm were obtained by solution casting techniques. The ULTEM® was dissolved in dichloromethane, $MeCl_2$, with small amounts of chloroform added in some cases.

Table 1
Typical properties of hydrophobically treated fumed silica used in this study

Fumed silica	Treatment	Density (g/cm^3)	B.E.T. surface area (m^2/g)	Particle size (nm)
TS610	Methyl	2.2	105–145	18.8–26.0
TS530	Trimethylsilyl	2.2	205–245	11.1–13.3
TS720	PDMS[a]	1.8	105–130	25.6–31.7

[a] The molecular weight of PDMS is about 10^3.

The polymer, solvent, and fumed silica were sheared for 10 min in a laboratory two-speed blender. The blended mixture was poured into flat Petri-dishes and covered to allow slow solvent evaporation. Thickness of the films was determined by a micrometer. Melt-processed nanocomposite membranes were also made by mixing in a DSM micro-extruder followed by compression molding. The polymer and fumed silica were mixed at 100 rpm for 3 min in the micro-extruder. The screw and barrel temperatures were set at 320 °C. The melt strand was transferred to a compression molder preheated to 320 °C to press the melt into films of about 200–300 μm thick. All samples were aged in a vacuum oven just below the glass transition temperature over night. The actual amount of fumed silica in each nanocomposite membrane was determined by burning the prepared membrane in a furnace at 900 °C for 45 min and measuring the residual fumed silica. All the samples used in this study are described in Table 2.

3.2. Measurements

The density of composite films was measured using a gradient column based on aqueous mixtures of calcium nitrate. Assuming volume additivity, the bulk density of the nanocomposite can be theoretically estimated from the composition and the known density of the components, i.e.,

$$\rho_{add} = \frac{1}{\frac{w_p}{\rho_p} + \frac{w_f}{\rho_f}} \tag{8}$$

Deviation from volume additivity can be expressed as an excess specific volume, ΔV, as follows

$$\Delta V = \frac{1}{\rho_m} - \frac{1}{\rho_{add}} \tag{9}$$

or as a volume fraction $\phi_{ex} = \Delta V \times \rho_m$, i.e.,

$$\phi_{ex} = \left[1 - \rho_m\left(\frac{w_p}{\rho_p} + \frac{w_f}{\rho_f}\right)\right] \tag{10}$$

where ρ_m is the measured density of the nanocomposite, ρ_p and ρ_f denote the measured densities of the pure polymer and the particles, respectively; w_p and w_f are the weight fractions of polymer and silica particles. The excess volume may reflect actual voids, particularly around particles or within

Table 2
Nanocomposite samples based on treated fumed silica [39]

Sample name	Fumed silica treatment	Preparation	Fumed silica content (wt%)	Fumed silica content (vol%)	T_g (°C)	d-Spacing
ULTEM		Solution-cast	0.00	0.00	206.7 ± 0.5	4.6
TS610-10	Methyl		10.1	6.33	206.4 ± 0.5	4.4
TS610-20			18.0	11.7	207.5 ± 0.3	4.4
TS610-30			27.4	18.5	207.9 ± 0.4	4.2
TS530-10	Trimethylsilyl		11.2	7.08	206.2 ± 0.3	4.4
TS530-20			20.8	13.6	207.3 ± 0.6	4.3
TS530-30			29.4	20.0	206.3 ± 0.1	4.2
TS720-10	PDMS		10.8	8.20	207.3 ± 0.4	4.6
TS610-20			20.7	16.0	207.7 ± 0.1	4.3
TS720-30			32.2	25.9	205.2 ± 0.1	4.2
ExULTEM		Melt-processed (DSM)	0.00	0.00	210.5 ± 0.2	4.8
ExTS610-3	Methyl		3.63	2.16	210.1 ± 0.2	–
ExTS610-17			17.3	10.9	210.3 ± 0.2	4.2
ExTS530-2	Trimethylsilyl		2.07	1.22	209.5 ± 0.2	–
ExTS530-11			11.8	7.26	209.0 ± 0.3	–
ExTS530-14			14.6	9.13	209.0 ± 0.2	4.5
ExTS720-2	PDMS		2.89	2.09	209.8 ± 0.2	–
ExTS720-6			6.16	4.49	209.3 ± 0.2	–
ExTS720-14			14.2	10.6	209.4 ± 0.3	4.2

agglomerates, a change in polymer free volume, or both. The density of the silica particles may have some level of uncertainty because the particles are small and have an organic coating on their surface. Differentiation of Eq. (10) leads to

$$d\phi_{ex} = \frac{\rho_m w_f}{\rho_f^2} d\rho_f \tag{11}$$

which provides a convenient way to assess the effect of errors in ρ_f on the calculated ϕ_{ex}. For example, at $w_f = 0.2$, if the error in ρ_f is ± 0.005 g/cm^3, then the error in ϕ_{ex} would be ± 0.0027. If the excess volume or ϕ_{ex} is of the order of 1%, then the error limits in this example would be nearly 30% for the ϕ_{ex} value. It will be useful to keep this in mind when examining these calculations.

The glass transition temperature (T_g) of the nanocomposite membranes was determined during heating in a Perkin–Elmer DSC-7 under a N_2 atmosphere. Samples sealed in an aluminum pan and then were heated from 50 °C to 300 °C at a scanning rate of 20 K/min two times. The T_g was calculated from the onset of the transition in the second scan.

Gas permeation through the nanocomposite assemblies was measured at 35 °C for He, O_2, N_2, CH_4 and CO_2 at an upstream pressure of about 28 psig (3 atm) by a constant volume/variable pressure type permeation cell frequently used in this laboratory and described in detail elsewhere [40,41]. The data can be represented as the amount of gas that has permeated, Q_t, as a function of time, t. Eventually, the plot of Q_t versus t becomes linear from which a steady-state permeability can be calculated as follows

$$P = \frac{dQ_t/dt}{A \times \Delta p/l} \tag{12}$$

where A and l represent the permeation area and membrane thickness, respectively, and Δp is the pressure driving force. When the downstream pressure is negligible relative to the upstream pressure, the separation factor or selectivity, α, can be written as a ratio of permeabilities:

$$\alpha_{AB} = \frac{P_A}{P_B} = \frac{(1-\phi)(P_0)_A f}{(1-\phi)(P_0)_B f} = \frac{(P_0)_A}{(P_0)_B} \tag{13}$$

where P_A and P_B are pure component permeabilities of A and B, respectively, and α_{AB} is the ideal permselectivity. According to composite theory, see Eq. (4), α_{AB} should not depend on the presence of particles or even voids around the particles so long as the voids do not traverse the entire membrane thickness.

Gas sorption measurements were carried out using a pressure decay method as a function of temperature in a dual volume apparatus described previously [42]. The effect of non-ideal gas behavior was accounted for by using compressibility factors [43].

Thin sections for transmission electron microscopy (TEM) ranging from 20 to 30 nm in thickness were cut with a diamond knife at a temperature of −40 °C using a Reichert-Jung Ultracut E microtome. In this process, the nanocomposite membranes were supported by epoxy resin to facilitate cutting. The sections were collected on 300 mesh square copper grids and subsequently dried with filter paper. The sections were examined by TEM using a JEOL 2010F TEM at an accelerating voltage of 120 kV.

A Hitachi S-4500 field emission scanning electron microscope (SEM) operated at a voltage of 15 kV was used to view cross-sections formed by cleaving the nanocomposite with tweezers after immersion in liquid nitrogen, subsequently coated with gold.

Wide angle X-ray diffraction scans were performed using a PHILIPS PW1720 X-ray generator at a scan rate of 1 °C/min

with Cu Kα X-ray radiation ($\lambda = 1.54$ Å) for pure polymer, fumed silica powder and nanocomposite membranes.

Uniformity of nanocomposite membranes obtained by solution casting was documented by photographs taken by a 4 megapixel digital camera, SONY Cyber-shot DSC-F77.

4. Results and discussion

4.1. Effects of solvent composition

To pursue the objectives of this research, it is necessary to be able to fabricate nanocomposite membranes in which the particles are well dispersed. Some reports suggest that application of ultrasonic energy to the casting solution facilitates good dispersion of the nanoparticles in the matrix [44]; however, this did not seem to improve film uniformity in this case. At the outset of this study, formulations containing fumed silica on hydrophobic treatments, TS530 and TS720, could not be formed into acceptable membranes by a single solvent such as methylene chloride ($MeCl_2$) because the fumed silica particles formed agglomerates and produced cracks [44,45]. However, we found that adding a slight amount of chloroform into $MeCl_2$ greatly assists in achieving composite membranes with good visual homogeneity. Fig. 2 documents that greatly improved nanocomposite membranes containing 30 wt% TS530 dispersed within ULTEM® could be formed by solution casting by adding just 2 vol% chloroform into the $MeCl_2$ solvent. The mechanism for this strongly beneficial effect of a small amount of chloroform in the casting solution most likely has to do with promoting wetting of the filler by the polymer. Clearly the chloroform restrains agglomeration of fumed silica within the ULTEM® matrix. For composite membranes containing TS530, especially, addition of 2–20 vol% chloroform to $MeCl_2$ enables the formation of homogeneous membranes. Interestingly, ULTEM®-based composite membranes containing any of the fumed silica (TS530, TS610 or TS720) cast from pure chloroform solvent were inhomogeneous. Composite membranes prepared by adding 2 vol% chloroform into $MeCl_2$ solvent were more transparent, had higher density and showed a more smooth surface than the composite membranes cast from pure $MeCl_2$ solvent. Thus, a mixed solvent of $MeCl_2$ plus 2 vol% chloroform was used for solution casting nanocomposite membranes in this study.

4.2. Physical properties

Table 2 shows the composition, glass transition temperature, T_g, and X-ray d-spacing of the various nanocomposites studied here as well as corresponding data for pure ULTEM®. There are slight variations in the T_gs observed. Solution-cast membranes tend to have a slightly higher T_g than pure ULTEM® while those made by melt processing tend to be even higher. The extensive drying protocol would seem to rule out the residual solvent as a significant source for reducing T_g. The WAXD patterns are essentially unchanged by the

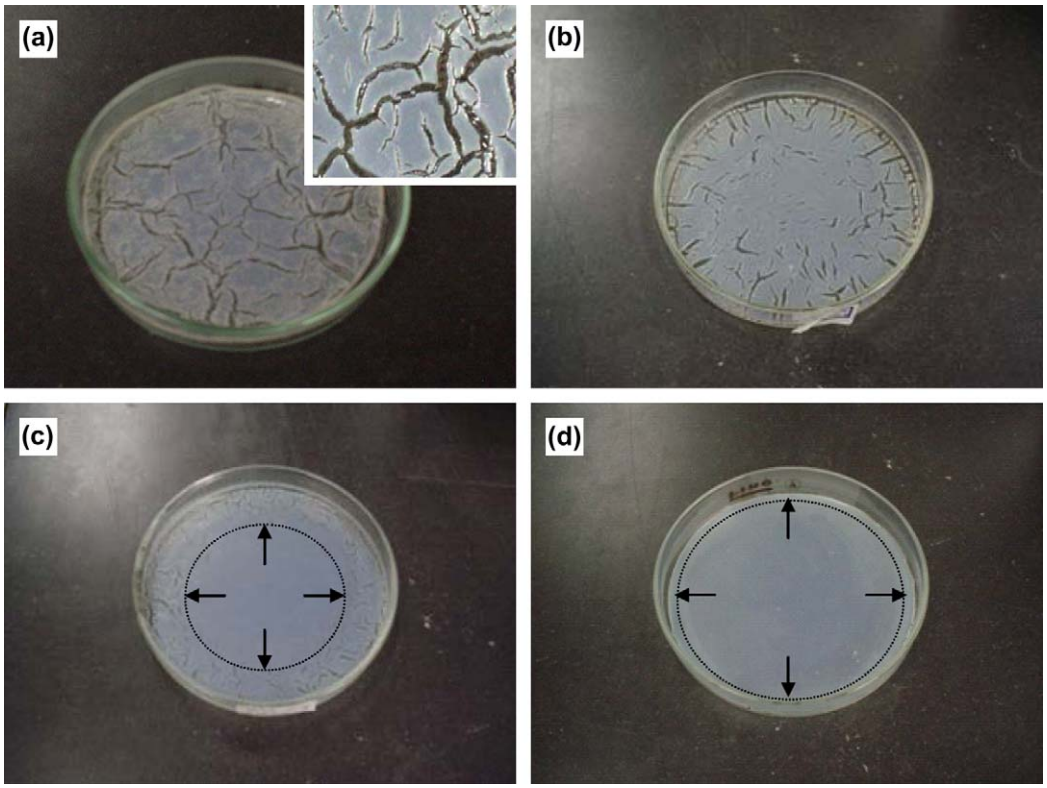

Fig. 2. Effect of addition of chloroform to the main casting solvent, methylene chloride ($MeCl_2$), on visual appearance and homogeneity of membranes containing fumed silica; photos show examples containing 30% of TS530. (a) $MeCl_2$ cast without any chloroform, (b) addition of 1 vol% chloroform to $MeCl_2$, (c) addition of 1.5 vol% chloroform to $MeCl_2$, and (d) addition of 2 vol% chloroform to $MeCl_2$.

presence of fumed silica in the composite. The slight variations in the *d*-spacings listed in Table 2 are probably not outside the experimental error limits.

4.3. Electron microscopy observation

Characterization by SEM and TEM provides some understanding of the morphology achieved. SEM micrographs of nanocomposite membranes made by solution casting are shown in Fig. 3 (images of free surface) and Fig. 4 (images of a cryofractured cross-section). Fumed silica with the TS610 treatment shows comparatively good dispersion at 20% loading as seen by the surface views in Fig. 3. However, the particles with surface treatments TS530 and TS720 exhibit considerable particle aggregation. The fumed silica with the long chain treatment (TS720) seems to be severely aggregated especially at higher fumed silica contents. The SEM images of cryofractured cross-sections shown in Fig. 4 make clear that fumed silica particles are not isolated filler particles but ''chains'' of particles fused together. These pictures demonstrate that adding fumed silica can lead to very heterogeneous morphologies. The nanocomposite membranes made by melt processing also showed similar morphologies by SEM observation.

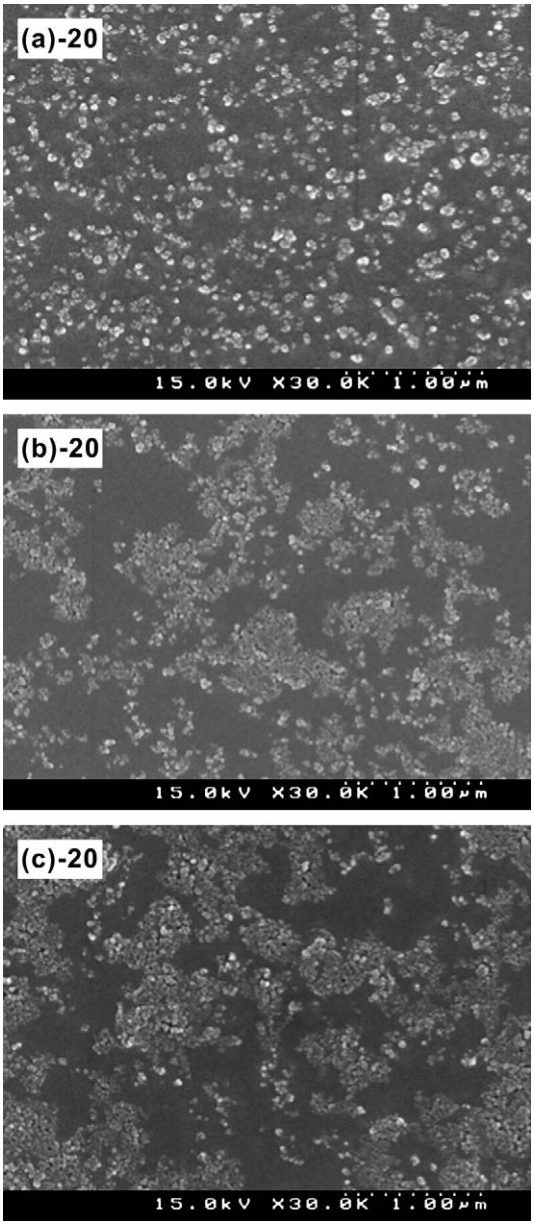

Fig. 3. SEM surface images of nanocomposite membranes containing fumed silica (20 wt% loading) with the following surface treatments (a) TS610, (b) TS530, and (c) TS720 prepared by solution casting.

TEM images of solution-cast membranes classified by fumed silica surface treatment and content are shown in Fig. 5. These images confirm the tendency of fumed silica particles to form agglomerates in the polymer matrix. Even the hydrophobic treatment based on methyl groups on the surface (TS610) leads to filler agglomeration. However, nanocomposites made by melt processing have relatively well-dispersed fumed silica in the matrix (see Fig. 6). At low fumed silica content, even TS720 with longer surface treatment chains seems well dispersed in the matrix.

4.4. Density characterization

The original objective of this research was to test the fundamental assumption of composite theory, that is, whether each phase in the composite has the same properties as if the other phase were not there. Ideally, the density of a composite should be predictable from the composition and the known density of the components as shown by Eq. (8). However, in real cases there may be non-additivity of volume such that the measured density deviates from that predicted by Eq. (8). In principle, the presence of the filler could alter the density of the polymer matrix and, hence, change its free volume [14]. On the other hand, such composites may form voids or defects around the filler particles especially when the filler forms agglomerates and wetting at the interface between matrix and filler is poor. We believe this is the dominant issue in the current systems. Density measurements are a convenient way to evaluate the extent of voids or gaps in the internal structure; TEM and SEM are not very useful for revealing such structural defects. In Fig. 7, the theoretical density calculated by Eq. (8) is shown by the dotted lines while the points show the measured density of the various nanocomposite membranes. The ULTEM®/TS720 theoretical line is lower than that of ULTEM®/TS610 or TS530 due to the lower density of TS720. The densities of nanocomposites formed from TS610 (methyl treatment) made by either solution casting or melt processing are closest to the theoretical line. However, the measured densities of composites containing TS530 or TS720 which have longer hydrophobic treatments on the fumed silica surface are lower than the theoretical line. The differences become larger with higher fumed silica loadings. Thus, the density observed depends on the kind or size of treatment on the fumed silica surface.

If the difference between the measured density and that computed by volume additivity is dominated by voids, as we believe, then the volume fraction calculated by Eq. (10) is

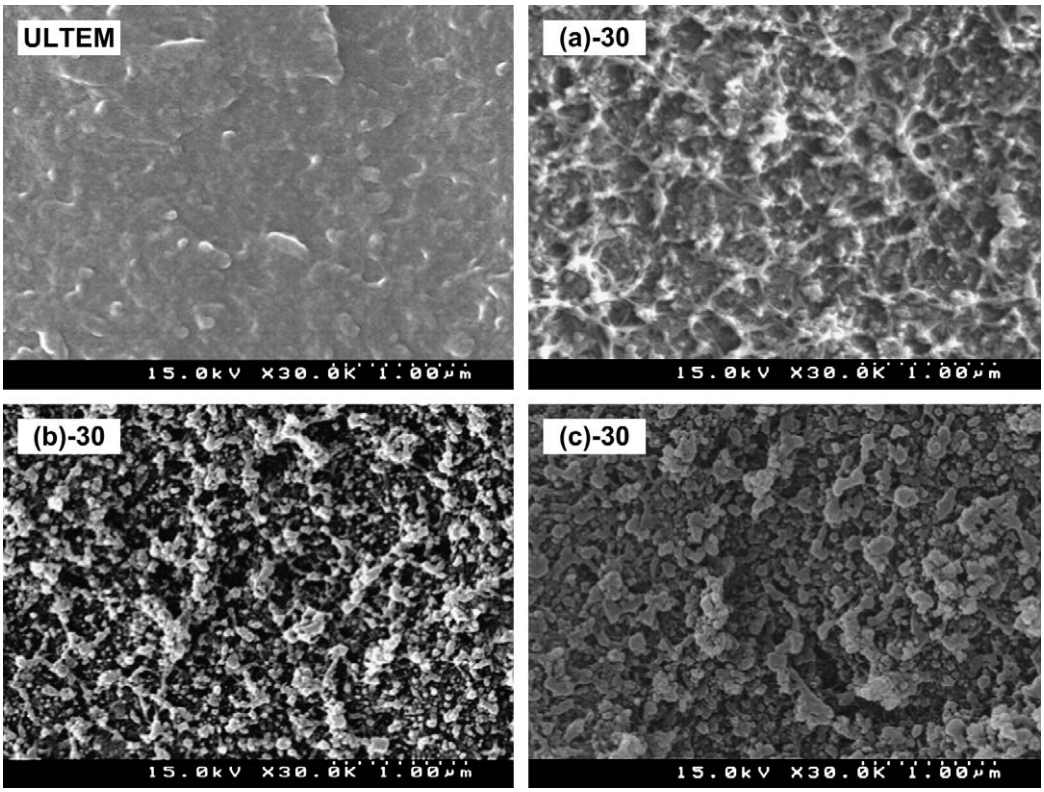

Fig. 4. SEM images of cryofractured cross-sections of pure ULTEM® and nanocomposite membranes containing 30% fumed silica with the following surface treatments (a) TS610, (b) TS530, and (c) TS720 prepared by solution casting.

a void volume fraction; see the current results in Fig. 8. The calculated void vol% increases with increasing fumed silica loading in all cases. The void content is strongly affected by the surface treatment on the fumed silica. However, for the nanocomposites made by melt processing, the void volume of the nanocomposite containing TS720 was less than that with TS530. In the case of solution casting, the addition of a small amount of chloroform to the casting formulation promotes wetting of the filler but apparently did not eliminate void formation on drying. It is important to recognize that the very large volume change associated with evaporation of the solvent apparently is a prime mechanism for void formation in such composites. Melt processing should remove this mechanism of void formation; however, thermal shrinkage, entrapped air, etc. represent other causes of void formation in this process.

According to the density measurements, the void content is small, 3% at most and as little as 0.2%, and varies depending on the surface treatment and processing methods. However, the effect of voids on gas permeability will depend on how the voids are distributed throughout the system; see Fig. 9 for several possible morphologies. In the present system, morphologies (c) and (d) in Fig. 9 seem more likely owing to the tendency of fumed silica particles to be fused together into ''chains'' [44,45]. The interconnectivity of voids could have a profound effect on gas permeability. However, so long as the voids do not form channels from one face of the membrane to the other, they should have no effect on selectivity.

4.5. Steady-state permeation properties

Fig. 10 shows example plots of gas permeability versus upstream driving pressure for large, CH_4 in Fig. 10(a), and small, He in Fig. 10(b), penetrant molecules as a function of upstream driving pressure for the pure polymer, ULTEM®, and composites, formed by solution casting, containing 30 wt% of fumed silica with the surface treatments described (see Fig. 1). For the pure polymer, the permeability is essentially independent of pressure for He and decreases slightly in the case of CH_4 as expected by the dual sorption model [41]. The composites show more or less similar pressure dependence as the neat ULTEM®; however, the absolute permeabilities are larger than for the neat polymer with the increase in permeability depending on the surface treatment on the fumed silica; the order of the increase is somewhat different for CH_4 than He.

Fig. 11 shows the oxygen permeability relative to that of pure ULTEM® (measured at 2 atm) of the various composites made by solution casting and melt processing techniques as a function of the volume fraction of fumed silica, ϕ. The prediction by Maxwell's theory is shown for reference by the dotted line. Clearly, the relative permeabilities are much higher for solution-cast than melt-processed membranes consistent with the void content shown in Fig. 8. Indeed, the void content is a broad predictor of the increase in permeability as shown later. The permeation behavior of the composites strongly depends on the nature of the surface treatment of the fumed

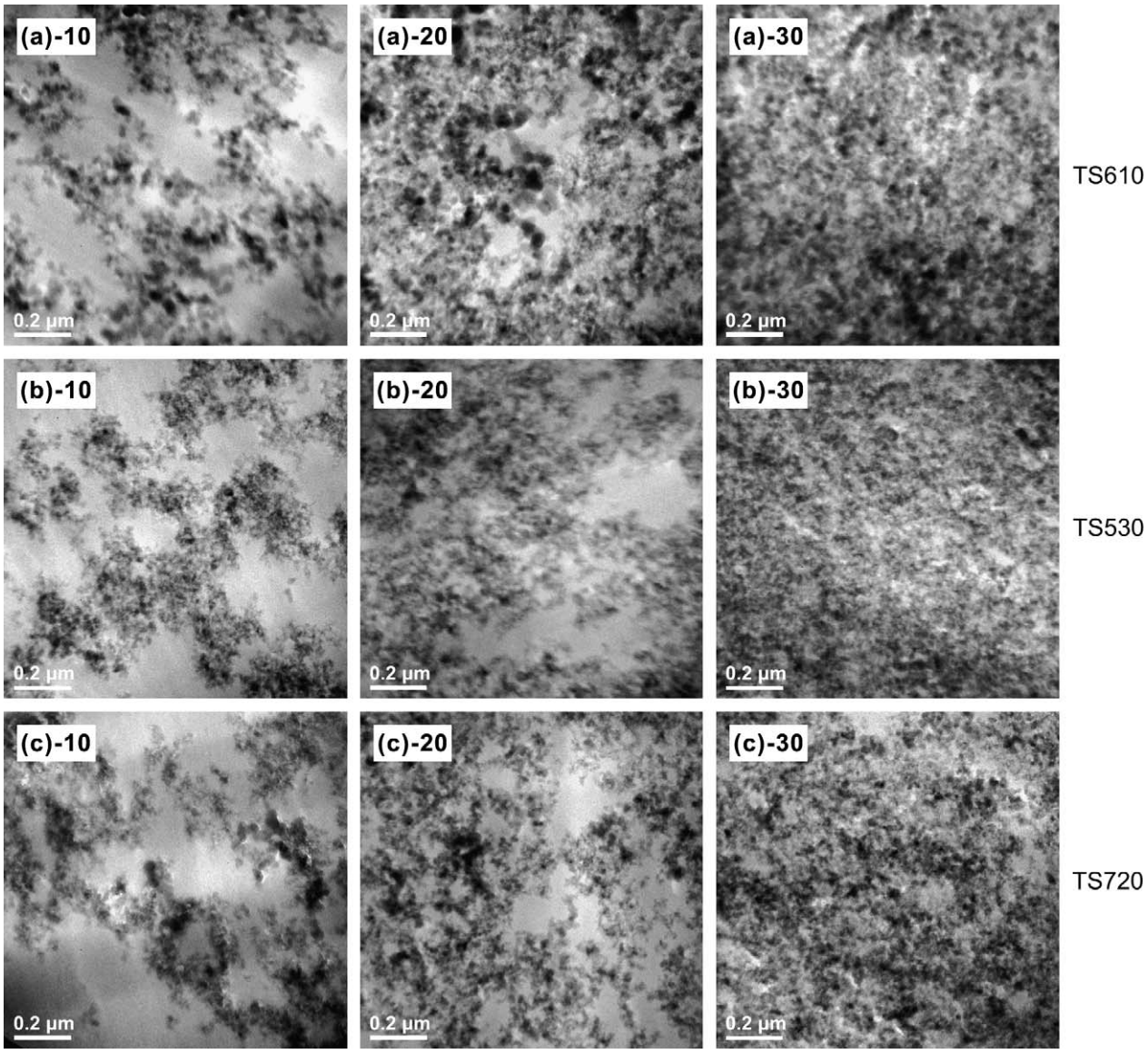

Fig. 5. A series of TEM images of nanocomposite membranes containing fumed silica made by solution casting: (a) TS610, (b) TS530, and (c) TS720. The numbers after the letters indicate the weight fraction of fumed silica. These images were taken at 15,000×.

silica. In all cases, the methyl treatment, TS610, causes the least increase in permeability regardless of the method of preparation.

The larger and more hydrophobic trimethylsilyl, TS530, and poly(dimethyl siloxane), TS720, surface treatments lead to considerably larger increases in oxygen permeability. The method of preparation seems to affect both the magnitude of the relative permeability and the influence of the surface treatment, see Fig. 11. Apparently, the wetting of particles is diminished as the surface becomes more hydrophobic.

As shown in Table 1, there are other differences in the fumed silica particle themselves in addition to their surface treatment. However, there seems to be no trend in particle size or B.E.T. surface area that would explain the trends for O_2 in Fig. 11 or for other gases, see Table 3. The surface treatment is believed to be the dominant factor.

For ideal composites without voids, the presence of the particles should have the same effect on the relative permeability for all gases as suggested by Eq. (4). Of course, if the particles affect the local properties of the matrix such that the assumptions behind this equation no longer apply, the gas type may affect the relative permeability, or selectivity, see Eq. (12), observed. Likewise, it can be argued that voids around particles as suggested by Fig. 9(b) and (c) should also lead to the same relative permeability regardless of gas type assuming that there is no effect of the particle on the local matrix properties. Thus, it is useful to compare the relative permeability for different gases in the various composites. This is done in Fig. 12 for the various solution-cast composites and in Fig. 13 for those made by melt processing. As discussed above, the relationship of the relative permeability versus volume fraction of filler is strongly affected by both the surface treatment and the

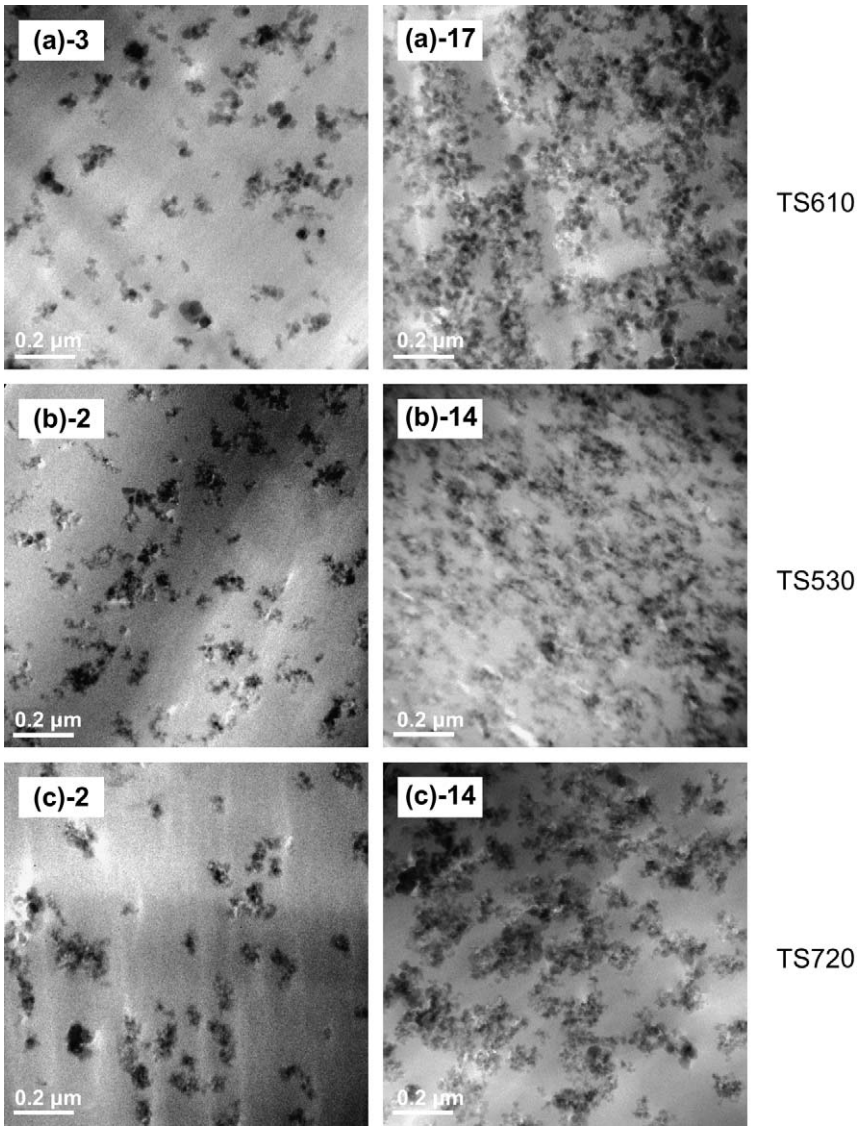

Fig. 6. A series of TEM images of nanocomposite membrane containing fumed silica made by melt processing at 320 °C: (a) TS610, (b) TS530, and (c) TS720. The numbers after the letters indicate the weight fraction of fumed silica. These images were taken at 15,000×.

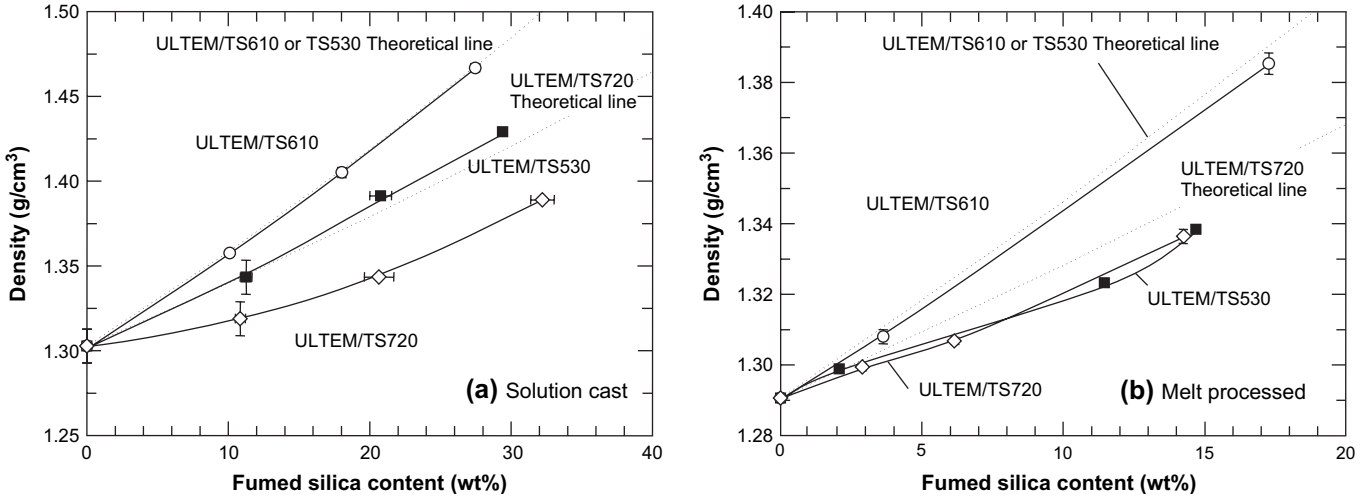

Fig. 7. Density of ULTEM®/fumed silica nanocomposites made by solution casting at 23 °C (a) and by melt processing (b) as a function of fumed silica content. The broken lines show theoretical predictions based on the pure ULTEM® density of 1.303 g/cm^3 and the density of each fumed silica, i.e., density of TS530 and TS610 is 2.2 g/cm^3 and that of TS720 is 1.8 g/cm^3.

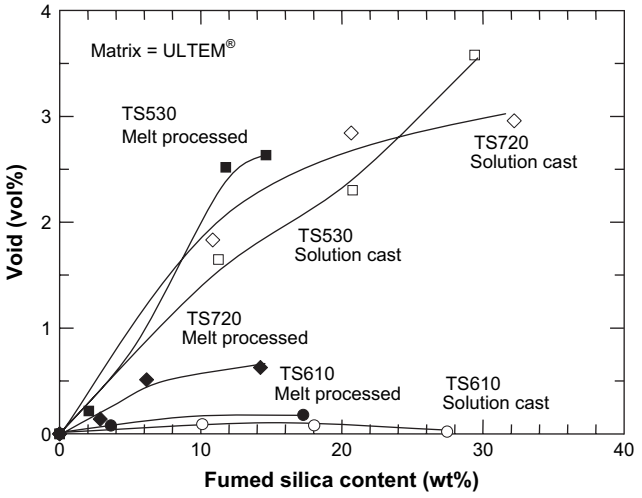

Fig. 8. Void volume fraction of ULTEM®/fumed silica nanocomposites made by solution casting and melt processing techniques as a function of fumed silica content. Void volume fraction was calculated by Eq. (11).

method of composite formation. However, the relative permeability also depends significantly on the gas type. In broad terms, the increase in relative permeability caused by addition of fumed silica particles increases as the permeability of the gas molecule in pure ULTEM® decreases, i.e., relative permeability generally ranks in the order $CH_4 > N_2 > O_2 > CO_2 >$ He; however, there are clearly exceptions for the composites with low void volume, especially those made from TS610 and those made by melt processing. A strict ordering of the relative permeability according to the ranking of permeability in pure ULTEM®, i.e., $CH_4 > N_2 > O_2 > CO_2 >$ He, suggests that permeation through the polymer matrix remains a dominant mode of transport; however, the decreased selectivity shown later suggests that there are interconnecting voids that traverse the entire membrane thickness, e.g., see Fig. 9(d). However, based on the results shown here, we cannot fully rule out the effects of the particle on the matrix local properties particularly for the cases where the void content is low.

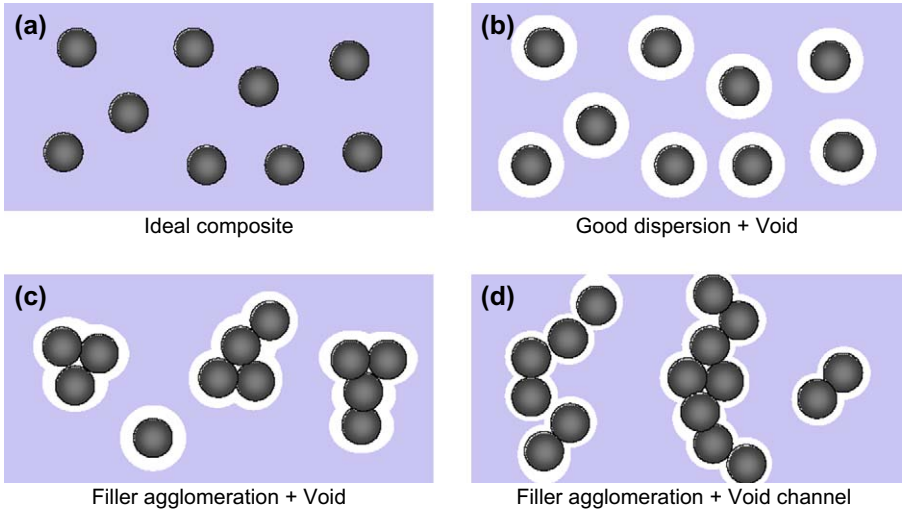

Fig. 9. Schematic illustrations of possible morphologies of composite membranes containing spherical filler particles including those that are partially fused together.

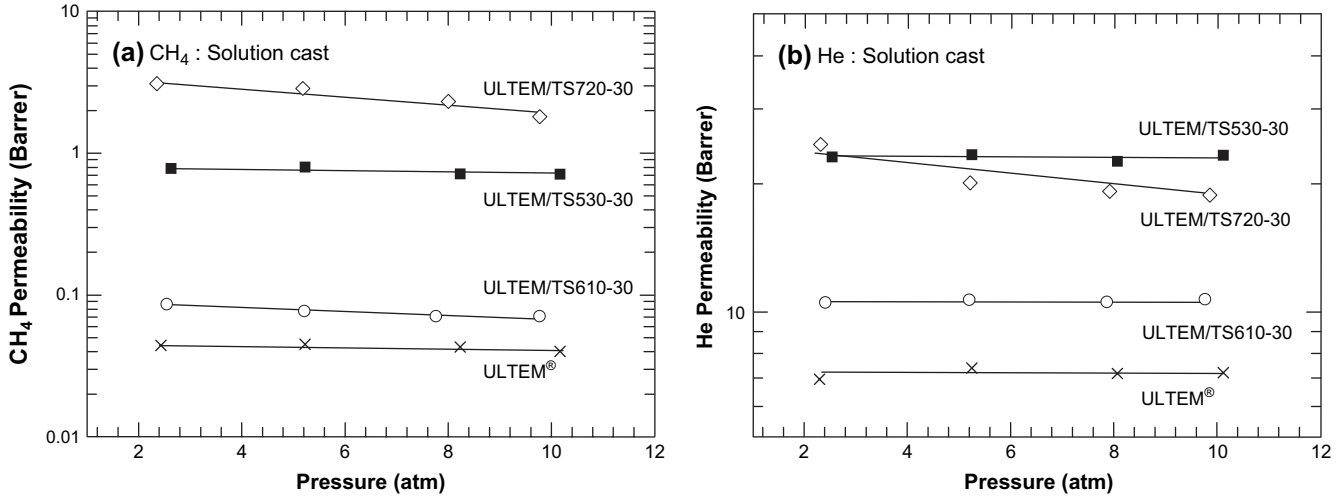

Fig. 10. Gas permeability coefficients for CH_4 (a) and He (b) in pure ULTEM® and nanocomposite membranes containing 30 wt% fumed silica made by solution casting.

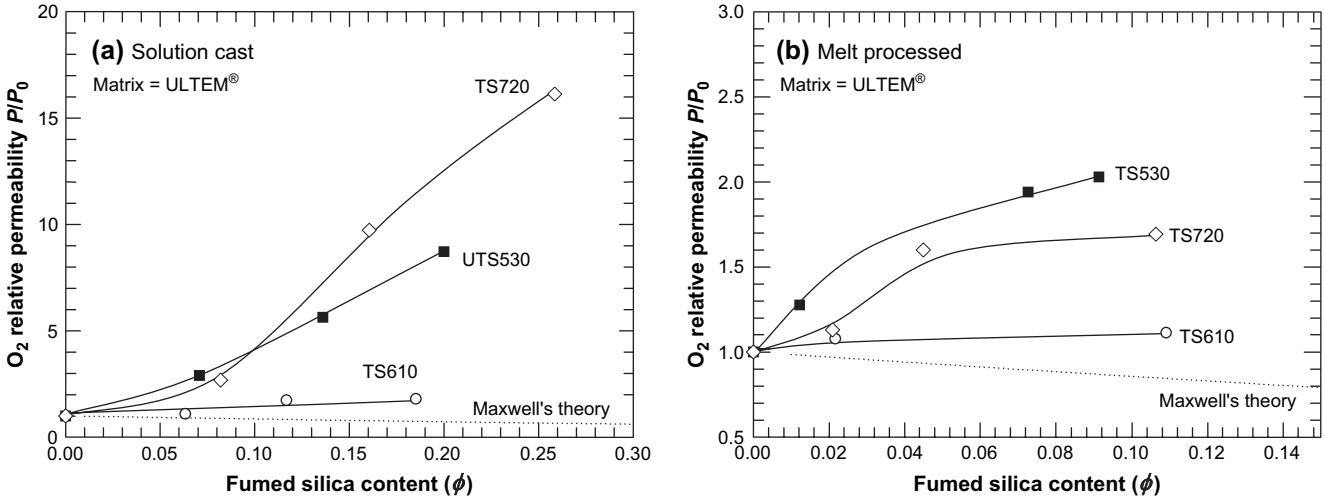

Fig. 11. Experimental relative permeability of oxygen in nanocomposites made by solution casting (a) and melt processing (b) as a function of fumed silica volume fraction. The prediction by the Maxwell's theory is shown for comparison.

In addition, the relative O_2 permeability is shown in Fig. 14 as a function of void volume fraction. There is a similar trend for all the gases used in this study. The relative permeability roughly correlates with the void volume. At the highest void fractions, around 3% or more, the relation becomes more scattered as might be anticipated as the tendency for interconnection of voids increases.

4.6. Time lag results

In addition to steady-state permeability, time lag measurements were made for some of the gases in the various fumed silica composites made by solution casting described earlier; the helium time lags were too short to be measured accurately. From the observed time lag, θ, and the membrane thickness, l, an apparent diffusion coefficient can be calculated as follows:

$$D_a = \frac{l^2}{6\theta} \tag{14}$$

Fig. 15 shows the apparent diffusivity coefficients normalized by the diffusion coefficient for that gas in ULTEM®, i.e., D_0 determined also from time lag data, as a function of fumed silica content. According to composite theory, Eq. (4), the relative diffusion coefficient should be independent of gas type and would be expected to decrease with the content of fumed silica owing to the tortuous path such impermeable particles

Table 3
Gas permeability coefficients and selectivities of composite samples used in this study

Sample name	Fumed silica treatment	Preparation	Permeability (Barrer)					$P(O_2)/P(N_2)$	$P(He)/P(CH_4)$	$P(CO_2)/P(CH_4)$
			He	O_2	N_2	CH_4	CO_2			
ULTEM		Solution-cast	6.95	0.34	0.05	0.04	1.32	6.75	158.	30.
TS610-10	Methyl		7.02	0.37	0.06	0.05	1.41	6.44	146.	29.
TS610-20			10.0	0.58	0.10	0.07	2.18	5.73	142.	30.
TS610-30			8.29	0.60	0.10	0.10	2.36	5.83	86.	25.
TS530-10	Trimethylsilyl		14.4	1.00	0.17	0.17	4.49	5.78	83.	26.
TS530-20			16.0	1.94	0.37	0.41	8.58	5.26	39.	21.
TS530-30			23.1	3.00	0.56	0.78	12.7	5.38	30.	16.
TS720-10	PDMS		11.6	0.92	0.19	0.24	5.42	4.79	49.	23.
TS610-20			23.0	3.35	0.79	1.37	13.5	4.21	17.	9.
TS720-30			24.7	5.55	1.50	3.09	21.6	3.71	8.	7.
ExULTEM		Melt-processed (DSM)	9.06	0.43	0.08	0.04	1.36	5.72	249.	37.
ExTS610-3	Methyl		8.98	0.46	0.08	0.03	1.43	5.73	270.	43.
ExTS610-17			8.74	0.48	0.09	0.04	1.39	5.33	236.	37.
ExTS530-2	Trimethylsilyl		10.7	0.55	0.10	0.06	1.82	5.73	190.	33.
ExTS530-11			12.3	0.84	0.16	0.11	2.88	5.20	114.	27.
ExTS530-14			13.16	0.87	0.15	0.11	3.19	6.03	124.	30.
ExTS720-2	PDMS		10.1	0.49	0.12	0.04	1.72	4.23	230.	39.
ExTS720-6			12.4	0.69	0.13	0.08	2.51	5.14	164.	33.
ExTS720-14			10.6	0.73	0.17	0.08	2.28	4.24	137.	30.

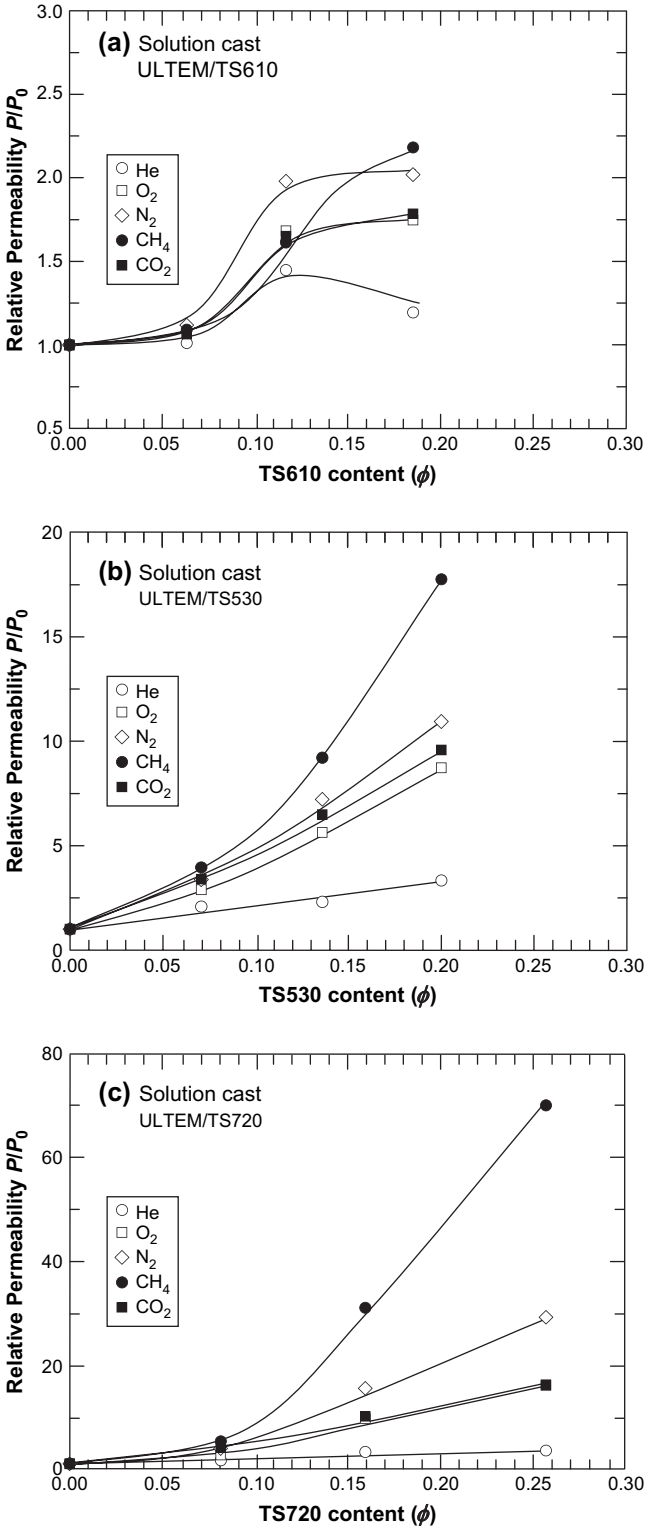

Fig. 12. Relative permeability of various gases in nanocomposites containing each kind of fumed silica made by solution casting as a function of fumed silica content. Measurements were carried out at 35 °C and at 3 atm: (a) ULTEM®/TS610, (b) ULTEM®/TS530, and (c) ULTEM®/TS720.

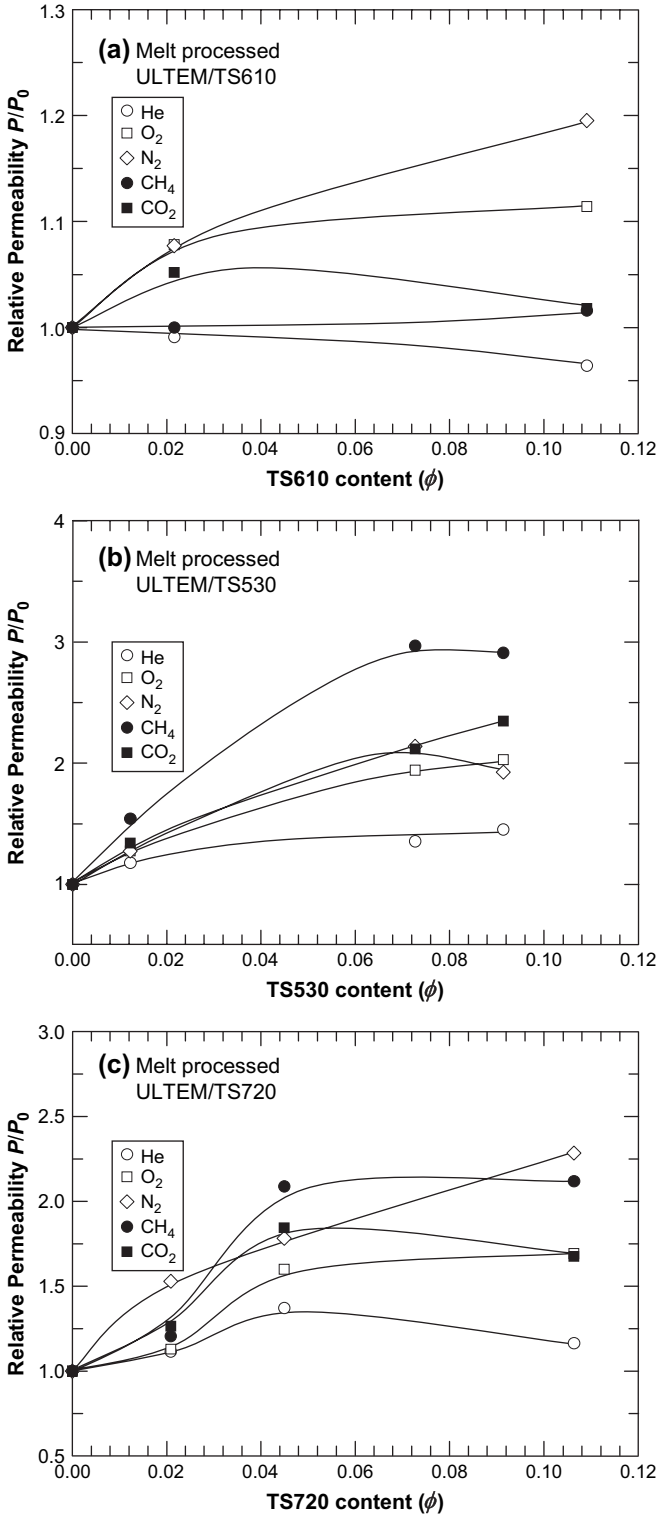

Fig. 13. Relative permeability of various gases in nanocomposites containing each kind of fumed silica made by melt processing at 320 °C as a function of fumed silica content. Measurements were carried out at 35 °C and at 3 atm: (a) ULTEM®/TS610, (b) ULTEM®/TS530, and (c) ULTEM®/TS720.

create. Instead, D_a/D_0 depends strongly on the gas type and always increases with the addition of silica particles. The extent of increase in D_a/D_0 depends strongly on the surface treatment on the silica particle, and, for the most part, the trends are quite similar as that of the relative permeability, P/P_0, shown in Fig. 12. Clearly, voids play a significant role in these results in creating a parallel pathway through the composite along with significant permeation through the matrix polymer.

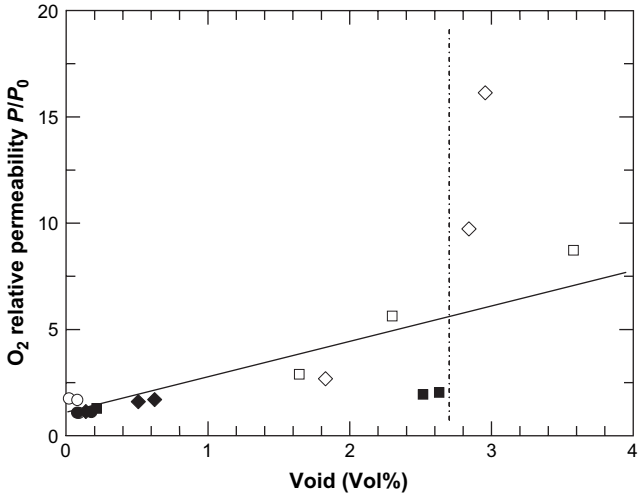

Fig. 14. Relationship between O_2 relative permeability and void volume fraction.

Again, some level of alteration of the properties of the matrix by the presence of the particles cannot be ruled out.

To the extent that Eqs. (1) and (14) apply for such complicated structures, one can calculate an apparent solubility coefficient as follows:

$$S_a = \frac{P}{D_a} \tag{15}$$

According to simple composite theory for non-sorbing particles, one expects the solubility of gases to decrease with the addition of filler as specified by Eq. (2). Fig. 16 shows the calculated solubility coefficients relative to that of pure ULTEM® for that gas. Complex trends are shown that depend on gas type, filler content, and surface treatment. Except in a few cases, the relative values, S_a/S_0, are greater than unity, contrary to simple expectations. Given the complexity of the results, it would be pointless to attempt a detailed interpretation of these trends. Clearly, the results reflect the presence of voids in addition to sorption in the matrix polymer plus possibly some contribution of adsorption by the filler or the filler/matrix interface [37,38].

To better understand this behavior, independent gas sorption experiments were carried out for CO_2 in pure ULTEM® and a solution-cast composite containing 30 wt% of each of the types of fumed silica, see Table 1 and Fig. 1, with the results shown in Fig. 17. The neat ULTEM® shows dual-mode type sorption behavior as expected for a glassy polymer [46]; the composites show similar type isotherms. However, each composite shows greater sorption than the matrix contrary to Eq. (2). The extent of sorption increase relative to the matrix depends somewhat on the surface treatment. While these trends are difficult to interpret, the excess sorption does not correlate with the relative permeability data in Fig. 12 or the relative apparent solubility data in Fig. 15. The excess sorption in Fig. 17 may be due to adsorption on the filler or at the filler–polymer interface, or may reflect an effect of the filler on the sorption characteristics of the ULTEM®.

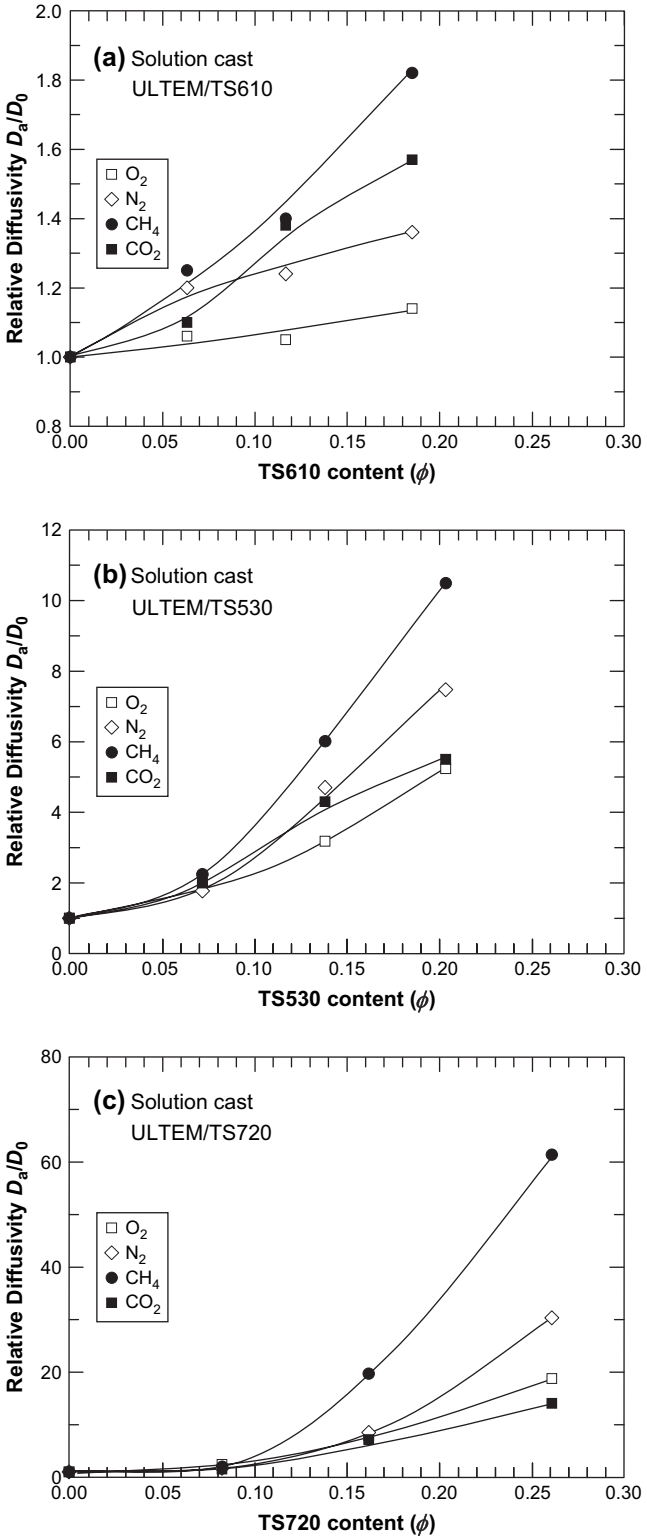

Fig. 15. Relative diffusivity of various gases in nanocomposites containing each kind of fumed silica made by solution casting as a function of fumed silica content. The diffusivity coefficients were computed from the observed time lags: (a) ULTEM®/TS610, (b) ULTEM®/TS530, and (c) ULTEM®/TS720.

Unfortunately, with the available equipment it was not possible to measure the CO_2 adsorption isotherm for the filler in the absence of ULTEM®.

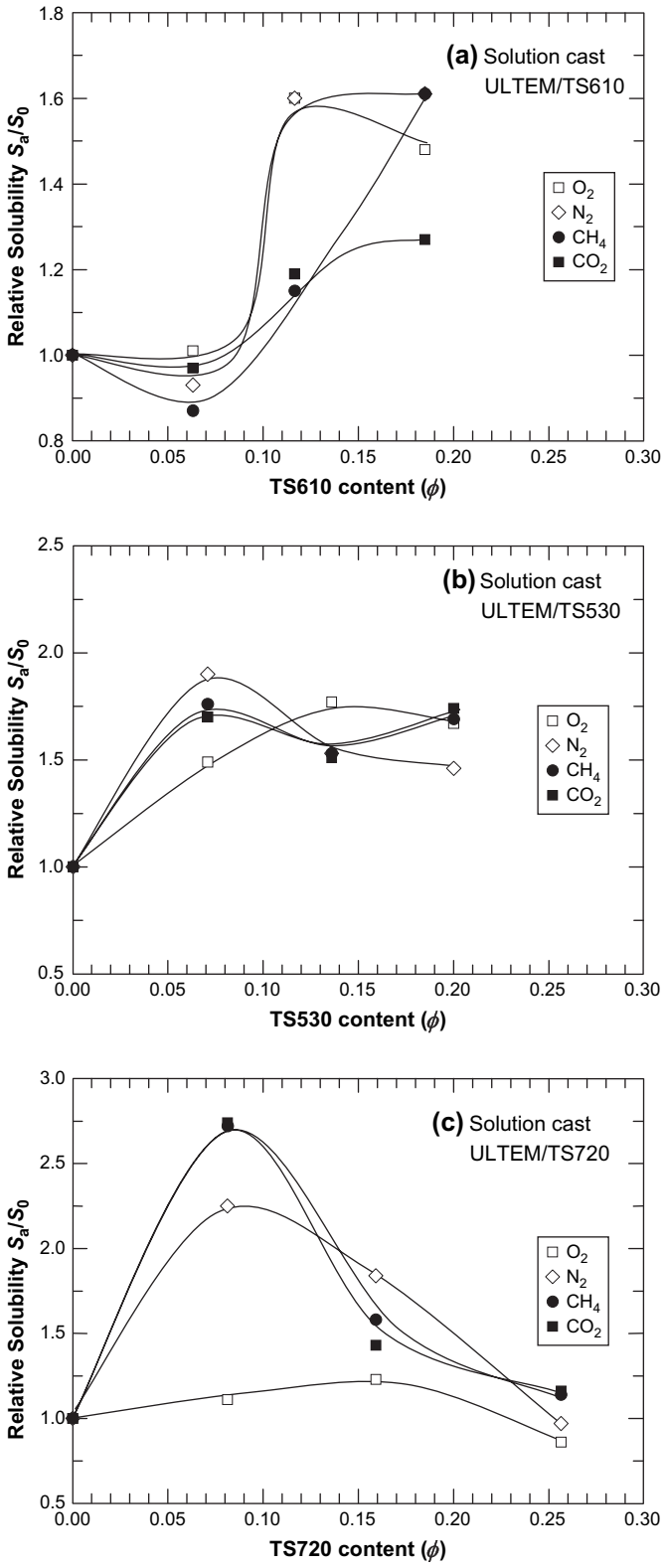

Fig. 16. Relative solubility of various gases in nanocomposites containing each kind of fumed silica made by solution casting as a function of fumed silica content. The solubility coefficients were calculated by dividing the experimental permeability by the diffusivity obtained from the time lag: (a) ULTEM®/TS610, (b) ULTEM®/TS530, and (c) ULTEM®/TS720.

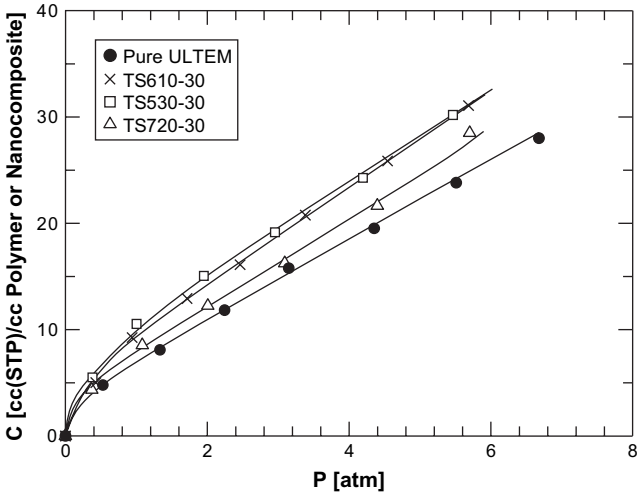

Fig. 17. Representative CO_2 sorption isotherms for pure ULTEM®, TS610-30, TS530-30 and TS720-30 made by solution casting at 25 °C.

4.7. Pure gas selectivity

Pure gas selectivities for various gas pairs, e.g., O_2/N_2, He/CH_4 and CO_2/CH_4, can be calculated from the steady-state permeability coefficients discussed above, see Table 3 and Fig. 18. In the absence of voids and any effect of the filler on the matrix, we expect these ratios to be independent of filler content and reflect the characteristics of the pure matrix, see Eq. (13), i.e., $(P_0)_A/(P_0)_B$. A similar result would also be expected if voids are present so long as the morphology is like that suggested in Fig. 9(b) or (c). In general, the trends in Table 3 and Fig. 18 indicate a reduction in selectivity, regardless of gas pair, as any one of the fumed silica materials is added to ULTEM®. This strongly suggests that a morphology like that in Fig. 9(d) probably exists to a certain extent. In general, the reduction in selectivity is greater for surface treatments that show greater void content (see Fig. 8) and greater increase in relative permeability (see Fig. 11). Interestingly, some finite level of selectivity is preserved indicating that permeation through the polymer is still a significant part of the permeation process, i.e., the voids do not totally dominate the permeation rate. Any effect of the filler on the matrix cannot be isolated because of the effect of the voids.

5. Conclusions

Previous papers have reported very interesting modifications to the gas permselectivity characteristics of several high free volume polymers by addition of high loadings of nanosized fumed silica particles that suggest modification of the physical state of the matrix polymer [14–21]. The objective of this work was to explore whether any analogous changes to gas permeability occur when the matrix is a more conventional (flexible chain) polymer. The amorphous, glassy poly(ether imide) sold commercially as ULTEM® was selected for this work. For the nanocomposites formed in this work, voids or defects at the polymer–particle interface

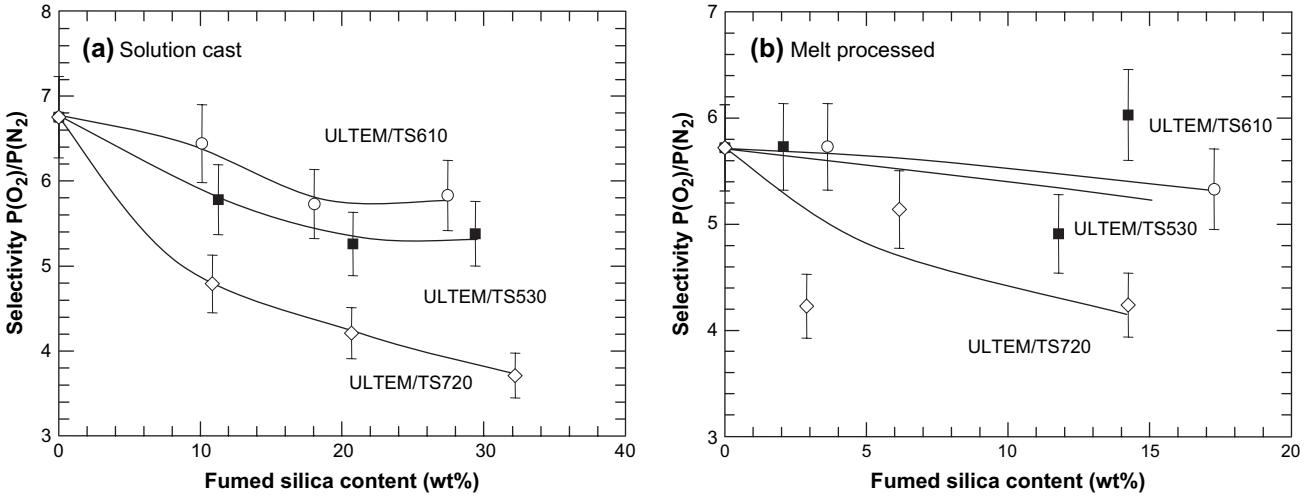

Fig. 18. O_2/N_2 selectivity in ULTEM®/fumed silica nanocomposites made by solution casting (a) and melt processing (b) as a function of fumed silica volume fraction.

became an overriding issue that had to be addressed. Three kinds of fumed silica with hydrophobic surface treatments were used but all led to severe particle agglomeration which combined with voids made the membrane have worse selectivity characteristics than the matrix polymer. Nanocomposite membranes were made by solution casting and melt processing techniques. Both TEM and SEM images showed the tendency of fumed silica particles to form agglomerates in the polymer matrix. In addition, the void volume as suggested from density measurements increased with fumed silica content in all cases. The void content is strongly affected by the surface treatment on the fumed silica; to some extent, there may be permeation through the thin layer of the surface treatment surrounding each particle but there seems to be no way to quantify this potential effect. Void content did not exceed 3% at most and was as low as 0.2% depending on the surface treatment and processing methods; however, these voids had significant effects on gas permeation behavior. The effect of voids on gas permeability depends on how the voids are distributed throughout the system. In all cases, the methyl treatment, TS610, causes the least increase in permeability regardless of the method of preparation. In most cases it appears that the voids create a parallel pathway through the composite along with permeation through the matrix polymer, see Fig. 9(d). The relative diffusivity obtained from time lag measurements also depends strongly on the surface treatment on the silica particle, and, for the most part, the trends are quite similar as that of the relative permeability. The apparent solubility coefficients calculated from the steady-state permeability and the apparent diffusivity from time lag measurements increase with filler content contrary to the expected result. However, measured sorption isotherms show excess sorption beyond that expected for the matrix polymer indicating possibly some contribution of adsorption by the filler or the filler/matrix interface. Also, a reduction in selectivity regardless of gas pair strongly suggests that the voids create small channels from one face of the membrane to the other. However, permeation through the polymer always makes a significant contribution to the selectivity of transport. Clearly, significant issues relating to the formation of nanocomposites from a conventional glassy polymer and hydrophobically treated fumed silica without concomitant formation of voids or defects must be solved before the original objectives of this work can be effectively explored. It was shown that some fumed silica treatments do minimize void formation and particle agglomeration. The second paper in this session seeks to eliminate interfacial voids or defects by the use of chemical reactions at the interface between matrix polymer and filler particles.

Acknowledgment

This work was supported by the National Science Foundation (Grant number DMR-0238979) and the Separation Research Program at the University of Texas at Austin.

References

[1] Mahajan R, Zimmerman CM, Koros WJ. Fundamental and practical aspects of mixed matrix gas separation membranes. In: ACS symposium series, vol. 733. Washington: American Chemical Society; 1999. p. 277–86.
[2] Mahajan R, Koros WJ. Mixed matrix membrane materials with glassy polymers. Part 1. Polym Eng Sci 2002;42:1420–31.
[3] Zimmerman CM, Singh A, Koros WJ. Tailoring mixed matrix composite membranes for gas separations. J Membr Sci 1997;137:145–54.
[4] Vu DQ, Koros WJ, Miller SJ. Mixed matrix membranes using carbon molecular sieves I. Preparation and experimental results. J Membr Sci 2003;211:311–34.
[5] Vu DQ, Koros WJ, Miller SJ. Mixed matrix membranes using carbon molecular sieves II. Modeling permeation behavior. J Membr Sci 2003; 211:335–48.
[6] Moore TT, Mahajan R, Vu DQ, Koros WJ. Hybrid membrane materials comprising organic polymers with rigid dispersed phases. AIChE J 2004; 50:311–21.
[7] Suer MG, Bac N, Yilmaz L, Gurkan T, Sacco Jr A. Gas separation with zeolite-based poly(ether sulfone) membranes. J Membr Sci 1994;91: 77–86.

[8] Duval JM, Kemperman AJB, Folkers B, Mulder MHV, Desgrandchamps G, Smolders CA. Preparation of zeolite filled glassy polymer membranes. J Appl Polym Sci 1994;54:409–18.
[9] Pechar TW, Tsapatsis M, Marand E, Davis R. Preparation and characterization of a glassy fluorinated polyimide zeolite-mixed matrix membrane. Desalination 2002;146:3–9.
[10] Vankelecom IFJ, van den Broeck S, Merckx E, Geerts H, Grobet P, Uytterhoeven JB. Silylation to improve incorporation of zeolites in polyimide films. J Phys Chem 1996;100:3753–8.
[11] DeGroot JV, Macosko CW. Aging phenomena in silica-filled polydimethylsiloxane. J Colloid Interface Sci 1999;217:86–93.
[12] Aranguren MI, Mora E, DeGroot JV, Macosko CW. Effect of reinforcing fillers on the rheology of polymer melts. J Rheol 1992;36:1165–82.
[13] Rong MZ, Zhang MQ, Zheng YX, Zeng HM, Walter R, Friedrich K. Structure–property relationships of irradiation grafted nano-inorganic particle filled polypropylene composites. Polymer 2001;42:167–83.
[14] Merkel TC, Freeman BD, Spontak RJ, He Z, Pinnau I, Meakin P, et al. Sorption, transport, and structural evidence for enhanced free volume in poly(4-methyl-2-pentyne)/fumed silica nanocomposite membranes. Chem Mater 2003;15:109–23.
[15] Merkel TC, Toy LG, Andrady AL, Gracz H, Stejskal EO. Investigation of enhanced free volume in nanosilica-filled poly(1-trimethylsilyl-1-propyne) by ^{129}Xe NMR spectroscopy. Macromolecules 2003;36:353–8.
[16] Merkel TC, Freeman BD, Spontak RJ, He Z, Pinnau I, Meakin P, et al. Ultrapermeable, reverse-selective nanocomposite membranes. Science 2002;296:519–22.
[17] Merkel TC, Freeman BD, He Z, Morisato A, Pinnau I. Nanocomposites for gas separation. Polym Mater Sci Eng 2001;85:301–2.
[18] Merkel TC, He Z, Pinnau I, Freeman BD, Meakin P, Hill AJ. Sorption and transport in poly(2,2-bis(trifluoromethyl)-4,5-difluoro-1,3-dioxole-*co*-tetrafluoroethylene) containing nanoscale fumed silica. Macromolecules 2003;36:8406–14.
[19] Zhong J, Lin G, Wen W, Jones AA, Kelman S, Freeman BD. Translation and rotation of penetrants in ultrapermeable nanocomposite membrane of poly(2,2-bis(trifluoromethyl)-4,5-difluoro-1,3-dioxole-*co*-tetrafluoroethylene) and fumed silica. Macromolecules 2005;38:3754–64.
[20] He Z, Pinnau I, Morisato A. Novel nanostructured polymer–inorganic hybrid membranes for vapor–gas separation. In: ACS symposium series, vol. 876. Washington: American Chemical Society; 2004. p. 218–33; see also U. S. Patent 6,316,684; 2001.
[21] Pinnau I, He Z, Morisato A. Nanostructured poly(4-methyl-2-pentyne)/silica hybrid membranes for gas separation. Polym Mater Sci Eng 2001;85:299–300.
[22] Tan Loon-Seng. Polymer data handbook. In: Mark JE, editor. New York: Oxford University Press; 1999. p. 471–8.
[23] Nunes SP, Peinemann KV, Ohlrogge K, Alpers A, Keller M, Pires ATN. Membranes of poly(ether imide) and nanodispersed silica. J Membr Sci 1999;157:219–26.
[24] Ghosal K, Freeman BD. Gas separation using polymer membranes: an overview. Polym Adv Technol 1994;5:673–97.
[25] Van Amerongen GJ. Diffusion in elastomers. Chem Technol 1964;37:1065–152.
[26] Maxwell JC. A treatise on electricity and magnetism, vol. 1. London: Oxford University Press; 1873.
[27] Lord Rayleigh. On the influence of obstacles arranged in rectangular order upon the properties of a medium. Philos Mag 1892;34:481.
[28] Nielsen LE. Models for the permeability of filled polymer systems. J Macromol Sci Chem 1967;A1:929–42.
[29] Lape NK, Nuxoll EE, Cussler EL. Polydisperse flakes in barrier films. J Membr Sci 2004;236:29–37.
[30] Perry D, Ward WJ, Cussler EL. Unsteady diffusion in barrier membranes. J Membr Sci 1989;44:305–11.
[31] Lape NK, Yang C, Cussler EL. Flake-filled reactive membrane. J Membr Sci 2002;209:271–82.
[32] Yang C, Smyrl WH, Cussler EL. Flake alignment in composite coatings. J Membr Sci 2004;231:1–12.
[33] Falla WR, Mulski M, Cussler EL. Estimating diffusion through flake-filled membranes. J Membr Sci 1996;119:129–38.
[34] Bharadwaj RK. Modeling the barrier properties of polymer–layered silicate nanocomposites. Macromolecules 2001;34:9189–92.
[35] Gusev AA, Lusti HR. Rational design of nanocomposites for barrier applications. Adv Mater 2001;13:1641–3.
[36] Fredrickson GH, Bicerano J. Barrier properties of oriented disk composites. J Chem Phys 1999;110:2181–8.
[37] Barrer RM, Barrie JA, Raman NK. Solution and diffusion in silicone rubber II. The influence of fillers. Polymer 1962;3:605–14.
[38] Barrer RM, Barrie JA, Rogers MG. Heterogeneous membranes: diffusion in filled rubber. J Polym Sci Part A 1963;1:2565–86.
[39] CAB-O-SIL TS-530, TS-610 and TS-720 treated fumed silica: technical data, Cabot Corporation; 2001.
[40] O'Brien KC, Koros WJ, Barbari TA, Sanders ES. A new technique for the measurement of multicomponent gas transport through polymeric films. J Membr Sci 1986;29:229–38.
[41] Barbari TA, Koros WJ, Paul DR. Gas transport in polymers based on bisphenol A. J Polym Sci Part B Polym Phys 1988;26:709–27.
[42] Koros WJ. PhD Dissertation, The University of Texas at Austin; 1977.
[43] Dymond JH, Smith EB. The virial coefficients of pure gases and mixtures: a critical compilation. New York: Oxford University Press; 1980.
[44] Sternstein SS, Zhu A. Reinforcement mechanism of nanofilled polymer melts as elucidated by nonlinear viscoelastic behavior. Macromolecules 2002;35:7262–73.
[45] Chakrabarti A. Effects of a fumed silica network on kinetics of phase separation in polymer blends. J Chem Phys 1999;111:9418–23.
[46] Koros WJ, Chan AH, Paul DR. Sorption and transport of various gases in polycarbonate. J Membr Sci 1977;2:165–90.